Structure of ordered and disordered α-brass

S. Müller and Alex Zunger
National Renewable Energy Laboratory, Golden, Colorado 80401
(Received 14 June 2000; published 5 February 2001)

Alloys of copper and zinc (brass) have been widely used since Neolithic times due to the discovery that unlike regular copper this alloy can be worked ''cold'' around a 3:1 copper-to-zinc ratio. While it is now known that the as-grown system is a disordered fcc solid solution, no 3:1 ordered phase has yet been directly observed even though the negative mixing enthalpy of the disordered alloy suggests ordering tendencies. Moreover, neutron scattering experiments have been deduced that this disordered alloy contains peculiar chains of Zn atoms. We have expressed the first-principles calculated total energy of general Cu-Zn fcc-lattice configurations using a mixed-space cluster expansion. Application of Monte Carlo–simulated annealing to this generalized Ising-like Hamiltonian produces the predicted low-temperature ground state as well as finite-temperature phase diagram and short-range order. We find (i) that at low temperature the disordered fcc alloy will order into the DO_{23} structure, (ii) the high-temperature short-range order in close agreement with experiment, and (iii) chains of Zn atoms in the [001] direction, as seen experimentally. Furthermore, our model allows a detailed study of the influence and importance of strain on the phase stability.

DOI: 10.1103/PhysRevB.63.094204 PACS number(s): 61.66.Dk, 61.43.Bn, 64.70.Kb, 71.15.Ap

I. INTRODUCTION

Alloys of copper and zinc (brass) have been widely used since Neolithic times when accidental mixing of copper and zinc ores was probably the reason for the discovery of its malleability, ductility, and ability to process even in cold conditions.[1–3] While it has been historically long known[3] that above 45% Zn (''white brass'') the alloy is not workable either hot or cold, at lower Zn concentrations brass is malleable. Near 50% Zn we have the phase now known[4] to have the disordered bcc structure (β-brass) above $\sim 460\,^{\circ}$C and the ordered CsCl structure at lower temperatures. Between 45% and 38% Zn we have the brass that can be worked only in hot conditions and is not very ductile, but is rather strong. This brass (currently used widely for manufacturing of decorative faucets) is now known as orthorombic 9R structure which can be formally derived from a face-centered tetragonal structure by introducing stacking faults on each third plane.[5] Below 38% Zn we have the historically most-widely used form of brass[1] that has excellent ''cold working'' properties and is ductile. This ''α-brass,'' which is the subject of this paper, is now known[4] to have at high temperatures the disordered fcc structure. Since it is known that the disordered bcc alloy (β) orders at low temperatures, it has long been suspected[6] that the disordered fcc alloy (α) will also order at lower temperatures. However, the ordered phase (which we might term α') was never detected, possibly due to a low order-disorder transition temperature $T_c^{\alpha\alpha'}$.

Although we know that α-brass is a disordered fcc alloy, there are definite clues that suggest that it is not a *random* alloy. First, measurements[7–9] of the mixing enthalpy of the alloy show that it is negative, suggesting the tendency of the Cu and Zn atoms to order crystallographically below some temperature $T_c^{\alpha\alpha'}$. Thus, immediately above this temperature one might expect nonrandom disorder. Second, measurements of the diffuse neutron scattering[10] of a sample quenched from high temperature ($T > T_c^{\alpha\alpha'}$) exhibit definitive deviations from randomness, manifested by peaks of the scattering around the $\langle 1\frac{1}{4}0\rangle$ and symmetrically equivalent positions in the Brillouin zone. Such peaks suggest that the disordered alloy is developing nonrandom composition waves which could signal its propensity to order crystallographically at lower temperatures. It is clear, however, from the short-range order (SRO) pattern that the structure that is being developed near $Cu_{0.75}Zn_{0.25}$ composition is *not* one of the fcc-ordered structures at the A_3B composition; for example, it is *not* the $L1_2$ structure characteristic of, e.g., Cu_3Au, Ag_3Mg, $AlPt_3$, or the DO_{22} structure characteristic of, e.g., $TiAl_3$, Ni_3V, Pd_3V. Finally, Reinhard *et al.*[10] noted that the high-temperature structure of their disordered alloy consists of unusual [001] chains with three to five Zn atoms

interpreted as an image of the Fermi surface along (110), then according to Reinhard *et al.*[10] $t=0.94$. Using this value and $e/a=1.25$ yields, using the Sato-Toth model, the ground-state structure with period $M\sim 2$. While highly suggestive, such Hume-Rothery concepts focus but on one piece of the total energy of the solid (the sum $\Sigma_i^{\epsilon_F}\epsilon_i$ of single-particle energies up to the Fermi level), neglecting interelectronic (Coulomb, exchange, and correlation) and ionic terms. Also, the atomic size-mismatch-induced strain (encoded in the full total energy) is neglected. It is important to emphasize that this approach does not predict the stable structure (out of many possible candidate configurations), but rather assumes it at the outset. Already early experimental studies[13,14] found deviations from ideal Hume-Rothery behavior in Cu-Zn; e.g., Mössbauer investigations[13] reported a stronger increase in the electron density of α-brass (fcc solid solution) than in that of β-brass (CsCl structure), when pressure is applied, while according to the Hume-Rothery rules the opposite should be true, because the number of outer electrons per atom is higher in β- than in α-brass.

More quantitative attempts to predict the structure of α- and α'

The first term $E_{pair}(\sigma)$ includes *all* pair figures, where $J_{pair}($

Cluster-Expansion of Cu-Zn (α-brass): 21 input structures

Average fit error (CE. 21 structures): 0.12 meV

Average prediction error (4 predictions*): 1.63 meV

Maximum error: 2.30 meV

Stoich.	x_{Zn}	Direction (100)	(110)	(111)	(201)	(311)	others	others
Cu direct: CE:	0.0						*fcc* 0.0 -0.1	
Cu_8Zn	0.111						Ni_8Nb_a -43.9 -43.5	
Cu_7Zn	0.125						*D7* -39.1 -39.3	
Cu_4Zn	0.20						$D1_a^*$ -66.2 -68.4	
Cu_3Zn	0.25	*Z1*	*Y1*	*V1*	$D0_{22}a$	*W1*	$L1_2$	

FIG. 1. Cluster expansion fit for α-brass. The compounds are sorted by superlattice direction and composition. Compounds marked by an asterisk are not input structures of the cluster expansion fit, but represents predictions. While the ''average fit error'' gives the standard deviation of cluster expansion formation enthalpies of input structures, the ''average prediction error'' represents the standard deviation of all predicted structures. The ''maximum error'' is the largest deviation between the cluster expansion and LDA values.

III. RESULTS

A. $T=0$ ground-state structure of fcc $Cu_{0.75}Zn_{0.25}$

Figure 2 shows the lowest-energy structure obtained by MC-simulated annealing of our LDA energy functional of Eq. (1), out of about $10^{15\,600}$ possible configurations. The structure can be identified as DO_{23} (Cu_6Zn_2), also pointed out by Reinhard *et al.*[10] and Turchi *et al.*[21] This structure is described in Table I. It can be viewed as a superlattice between $L1_2$ and a translated $L1_2$ structure ($L1_2'$), shown in Fig. 3: DO_{23} can be constructed from $L1_2$ by forming an antiphase boundary after every two lattice constants in [001] direction; i.e., the modulation period M of the structure with respect to $L1_2$ is $M=2$. This modulation wavelength can be noted by viewing our ground-state structure as shown in the lower part of Fig. 2. Table II compares the pair- and multibody-correlation functions found by our ground-state search and those for an ideal DO_{23} structure. They are identical, proving that the found ground-state structure is indeed DO_{23}. This predicted structure was not observed experimentally as an ordered phase in Cu_3Zn, presumably because it disorders at low temperatures (see Sec. III D).

B. Energetic stability of the $T=0$ ground state and its competing structures

Our calculation reveals delicate energy balance between the various Cu_3Zn competing phases:

$$M=0,\ \Delta H(\text{random})=-55.0\ \text{meV/atom},$$

$$M=1,\ \Delta H(\text{DO}_{22})=-77.1\ \text{meV/atom},$$

$$M=2,\ \Delta H(\text{DO}_{23})=-88.1\ \text{meV/atom},$$

$$M=3,\ \Delta H(\text{LPS3})=-87.2\ \text{meV/atom},$$

$$M=\infty,\ \Delta H(L1_2)=-87.4\ \text{meV/atom}. \quad (8)$$

We see that the energy difference between DO_{22} ($M=1$) and $L1_2$ ($M=\infty$) amounts to only 11 meV/atom. Turchi

et al.[21,22] used the lowest order in the generalized perturbation method (GPM) to calculate the energy difference between the simplest LPS, DO_{22}, and $L1_2$. The model was restricted to six pair interactions and no multibody interactions were taken into account, leading to an energy difference of about 24 mJ/m^2 (Ref. 22) between $L1_2$ and DO_{22}. Our corresponding LDA value is 22.8 mJ/m^2, in excellent agreement with the GPM result.

Since the formation enthalpies for $M=2,3$

TABLE II. Pair- and multibody-correlation functions resulting from the ground-state search for $Cu_{0.75}Zn_{0.25}$ via Monte Carlo annealing. As can be seen, the values found are identical to those of DO_{23}, identifying this compound as low-temperature ground of α-brass.

PAIR-IA	$\Pi_i^{pair}(DO_{23})$	$\Pi_i^{pair}(MC)$	MB-IA	$\Pi_i^{mb}(DO_{23})$	$\Pi_i^{mb}(MC)$
J_1	0.0000	0.0000	$J3$	0.5000	0.5000
J_2	0.8333	0.8333	$K3$	−0.3333	−0.3333
J_3	0.1667	0.1667	$L3$	0.3333	0.3333
J_4	0.6667	0.6667	$M3$	−0.5000	−0.5000
J_5	0.0000	0.0000	$J4$	−1.0000	−1.0000
J_6	0.5000	0.5000	$K4$	−0.1667	−0.1667
J_7	0.1667	0.1667	$L4$	−0.8333	−0.8333
J_8	0.6667	0.6667			
J_9	0.0000	0.0000			
J_{10}	0.3333	0.3333M3g8.98 0 1.0.8333			

temperature ground state of α-brass, the discussion above makes clear that a consideration of fewer than ten pair interactions would lead to an incorrect answer: $L1_2$ would then be the low-temperature ground state of Cu_3Zn, in disagreement with experimental SRO studies.[10] Furthermore, we see that a consideration of at least 15 pair interactions is necessary to reach convergence in the energy differences between the structures with $M=2$, $M=3$, and $M=\infty$. Actually, the consideration of such a large number of interactions distinguish our approach from earlier theoretical investigations[15,16,20–22] on α-brass.

C. Comparison of $T=0$ long-period structures of Cu_3Zn and Cu_3Pd

Figure 6 compares the energies of the long-period superlattices E_M vs M for Cu_3Zn and Cu_3Pd. Values for Cu_3Pd are taken from Lu *et al.*[36] In excellent agreement with the LDA calculated formation enthalpies of Cu_3Zn (shown as open squares) our prediction locates a minimum for $M=2$, corresponding to the DO_{23} structure. Lu *et al.*[36] found for

Cu_3Pd the $M=3$ structure as the most stable structure of the LPS group. It is interesting to note that following the work by Sato and Toth,[12] a modulation wavelength $M=4$ is expected for Cu_3Pd instead of the LDA value $M=3$: The use of a ratio $t=0.94$ (already introduced in Sec. I) and $e/a=0.75$ for Cu_3Pd gives $e/a=0.70$ for $M=3$, but $e/a=0.74$ for $M=4$.

Since in Cu_3Zn the $T=0$ stable structure is $M=2$, whereas in Cu_3Pd it is $M=3$, we expect to see ''fingerprints'' of these differences on the SRO diffuse scattering. Since the fundamental reciprocal space wave vector of long-periodic superlattices is given by $\mathbf{k}=\langle 1\ 1/2M\ 0\rangle$ with M being the modulation wavelength (see, e.g., Refs. 36 and 37), SRO peaks should appear at different positions in the diffuse scattering patterns of Cu_3Zn and Cu_3Pd. While Cu_3Zn with DO_{23} ($M=2$) as ground state should show SRO intensities at $\mathbf{k}=\langle 1\,\frac{1}{4}\,0\rangle$ and symmetrtically equivalent positions (in agreement with the observation), Cu_3Pd with LPS3 ($M=3$) as ground state should show SRO intensities at $\mathbf{k}=\langle 1\,\frac{1}{6}\,0\rangle$ and symmetrtically equivalent positions. This is discussed in Sec. III E.

D. Finite-temperature boundary between the ordered low-temperature structure α' and the disordered alloy α

We next study finite-temperature effects. The solid line in Fig. 7 shows our calculated phase diagram, delineating the ordered $M=2$ superlattice from the disordered alloy. This phase boundary can be identified by Monte Carlo–simulated annealing, recording the specific heat c_V as a function of temperature. Being the response function of the energy, c_V has a maximum at the critical temperature T_c. Repeating the annealing process for different concentrations leads to the ordered

$$\delta E_{ord(no\text{-}strain)} = [\Delta H_{DO_{23}} - E_{CS}(DO_{23})] - [\Delta H_{SQS14a} - E_{CS}(\mathrm{SQS14}a)] = -39.4 \text{ meV/atom.}$$

So neglecting strain leads to a more negative ordering energy and, therefore, to a more stable DO_{23} structure. Consequently, the coherent phase boundary will shift to higher temperatures.

E. Short-range order diffuse scattering in the high-temperature disordered α-brass

Having calculated the $T=0$ stable phase of Cu_3

important. For $x_{Zn}=0.20$, the SRO peaks are no longer exactly on $[1\frac{1}{4}0]$ positions, but are displaced to $[1\frac{1}{6}0]$. This could be a consequence of ''missing'' Zn atoms (concentration is smaller than 25%) so that on the average the modulation wavelength M has to be increased and, therefore, the SRO peaks are shifted towards the X

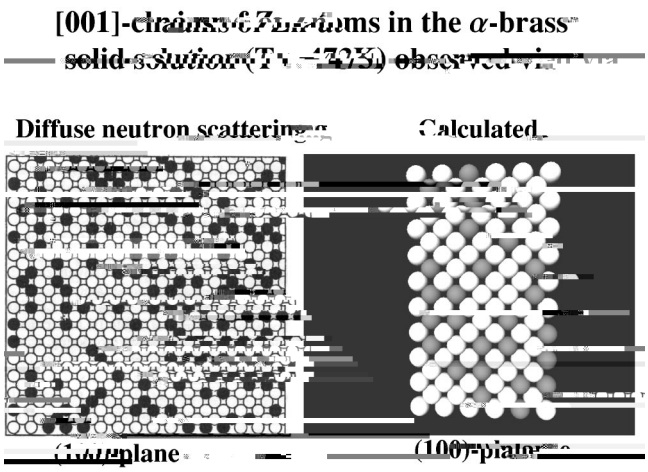

FIG. 12. Visualization of a (100) plane of α-brass (cut through the crystal) for $T=473$ K. While the left picture results from a model crystal based on diffuse neutron scattering experiments (Ref. 10), the right picture is the result of MC simulations using ΔH_{CE}. In both cases, chains of Zn atoms along [001] can be seen, indicating that SRO is present and, therefore, the observed solid solution cannot be described by a random alloy.

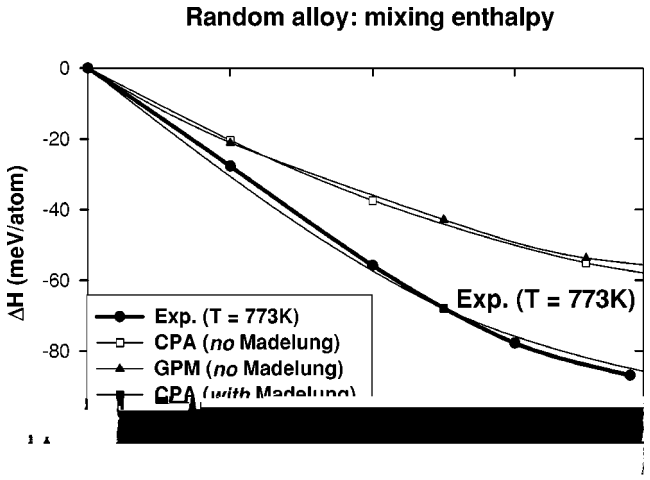

FIG. 13. Comparison of mixing enthalpies resulting from experiment (Ref. 4) 211111111111ng temperatures, sta Ref. 4) 1611111111111ng ten

with that obtained from the Monte Carlo simulations of our LDA cluster expansion. Unlike our calculation, the pattern resulting from the concentration wave calculation shows a number of satellite spots around $\mathbf{k}=\langle 1\pm\epsilon,\ \sim\frac{1}{4},\ 0\rangle$ which might lead at low temperatures to ordering of a different structure than we find $(\mathrm{DO}_{23};M=2)$. Unfortunately, Turchi *et al.*[21] did not anneal their alloy in order to determine the corresponding ground-state structure, so a direct comparison with our predicted low-temperature phase is not possible.

F. Appearance of Zn chains in α-brass

Real-space imaging of the measured SRO in high-temperature quenched α-brass showed [001] chains of Zn atoms.[10] As discussed by Reinhard *et al.*,[10] these chains are a direct consequence of the observed SRO behavior of the system: While all SRO parameters described by $(lmn)=(2n;0;0)$ are positive (see Table III), all SRO parameters described by $(2n-1;1;0)$ are negative. This should lead to chains of Zn atoms along the [001] direction. The authors studied this assumption using an fcc model crystal which was fitted to the experimental SRO parameter of Table III. Figure 12 gives a comparison between the real-space structure deduced from experiment[10] and from our parameter-free model: In both cases, chains of Zn atoms are visible along [001], indicating that short-range order is essential for a quantitative correct description of the physical properties of the disordered solid solution of α-brass.

G. Effect of SRO on the mixing enthalpy

Figure 13 compares experimental mixing enthalpies as function of Zn concentration with earlier theoretical studies for the random alloy; i.e., no SRO is taken into account. The experimental values were taken from Ref. 4 and were measured at $T=773$ K. As discussed in the Introduction, Fig. 13 clearly shows that charge transfer is making a big effect on the results. It can be seen that the corrected CPA of Johnson and Pinski[20] agrees very well with experiment, although SRO is neglected in the calculation. In order to study the influence of SRO on the mixing enthalpy, Fig. 14 compares $\Delta H_{mix}(x,T)$ for different temperatures, starting from the random alloy $(T\rightarrow\infty)$ and cooling down to temperatures where SRO sets in. Comparing the energy curves for the random and the disordered alloy, we see that the calculation neglecting SRO leads to much higher mixing enthalpies. Moreover, it can be seen that especially for higher Zn concentrations good agreement between experiment and calculated mixing enthalpies can only be reached, if SRO is taken into account. We do not have an explanation why the CPA calculations shown in Fig. 13 lead to reasonable mixing enthalpies without consideration of SRO.

The observed decrease of ΔH_{mix} with decreasing temperature can be discussed in terms of individual effective

cluster interactions. For this purpose, we chose a concentration $x_{Zn}=0.3$ and study the contribution of each cluster probability $\overline{\Pi}_f$ as a function of temperature. Going back to Fig. 4(b), we see that the first pair interaction $J_1>0$ is ''antiferromagnetic'' (Cu-Zn attraction) while the second and third interactions $J_2, J_3<0$ are ''ferromagnetic'' (Cu-Zn repulsion). We find that the decrease in ΔH_{mix} with decreasing temperature is caused by the elimination of the first-neighbor pairs ($\overline{\Pi}_1 \rightarrow 0$) and enhancement of second-neighbor pairs ($\overline{\Pi}_2$

perature appears at relatively low temperatures which is